The Effect of Modeling Assumptions on the ECG in Monodomain and Bidomain Simulations

Dennis Ogiermann[1]([✉]) [ID], Daniel Balzani[1] [ID], and Luigi E. Perotti[2] [ID]

[1] Chair of Continuum Mechanics, Ruhr-University Bochum, Bochum, Germany
dennis.ogiermann@ruhr-uni-bochum.de
[2] Mechanical and Aerospace Engineering Department, University of Central Florida, Orlando, FL, USA

Abstract. Computing a physiologically accurate electrocardiogram (ECG) is one of the key outcomes of cardiac electrophysiology (EP) simulations. Indeed, the simulated ECG serves as a validation, may be the target for optimization in inverse EP problems, and in general allows to link simulation results to clinical ECG data. Several approaches are available to compute the ECG corresponding to an EP simulation. Lead field approaches are commonly used to compute ECGs from cardiac EP simulations using the Monodomain or Eikonal models. A coupled passive conductor model is instead common when the full Bidomain model is adopted. An approach based on solving an auxiliary Poisson problem propagating the activation field from the heart surface to the torso surface is also possible, although not commonly described in the literature. In this work, through a series of numerical experiments, we investigate the limits of validity of the different approaches to compute the ECG from simulations based on the Monodomain and Bidomain models. Significant discrepancies are observed between the common lead field and direct ECG approaches in most realistic cases – e.g., when conduction anisotropy is included – while the ECG computed via solution of an auxiliary Poisson problem is similar to the direct ECG approach. We conclude that either the direct ECG or Poisson approach should be adopted to improve the accuracy of the computed ECG.

Keywords: Electrocardiogram · Cardiac electrophysiology · Validation criteria · Monodomain model · Bidomain model

1 Introduction

Validation of mathematical models in cardiac electrophysiology is a challenging task, which gained significant attention over the last years. Indeed, satisfying verification and validation criteria is a critical step necessary to translate mathematical models and the respective numerical simulations to clinical practice. Once validated, EP simulations have a vast range of applications from personalized medicine to drug development. Our goal is to move one step further towards

unlocking these applications by investigating commonly used methods to compute electrocardiograms (ECGs) in numerical studies. The ECG is one of the most widely used diagnostic tools in cardiology for its low cost, simplicity, and amount of information provided on cardiac function and disease. Given its wide adoption and significant relevance in the clinical practice, the ECG is one of the key validation criteria to be satisfied by an EP simulation, while simultaneously respecting physiological activation sequences [9].

The contribution of the current study towards reaching this milestone is to carefully review commonly adopted modeling assumptions to compute the ECG from EP simulations and to highlight discrepancies and their causes. Particular attention will be given to evaluating the lead field approach due to its common use in the literature. Preliminary analyses comparing the lead field approach and the direct ECG have been carried out in [12], while [3] investigated the effect on the ECG of different coupling models between the torso and the heart. In this work we continue this effort with an in depth analysis comparing the lead field approach and directly computed ECGs.

2   Methods

Cardiac electrophysiology and the ECG are commonly simulated using the Monodomain model together with the lead field approach (to recover the ECG) [14]. In comparison, fewer studies solve the Bidomain equations [16] coupled with a passive conductor model for the torso, where the extracellular potential is tied at the torso-heart interface. In this case the ECG is directly computed from the extracellular potential on the surface of the torso.

2.1   Direct ECG

The Bidomain model [16] coupled to a surrounding passive conductor can be stated in parabolic-elliptic form as:

$$
\chi C_{\mathrm{m}} \frac{\partial \varphi_{\mathrm{m}}}{\partial t} = \nabla \cdot (\boldsymbol{\kappa}_{\mathrm{i}} \nabla \varphi_{\mathrm{m}}) + \nabla \cdot (\boldsymbol{\kappa}_{\mathrm{i}} \nabla \varphi_{\mathrm{e}}) - \chi I_{\mathrm{ion}}(\varphi_{\mathrm{m}}, \mathbf{s}) - \chi I_{\mathrm{stim}}(t) \quad \text{in } \Omega_{\mathbb{H}}
$$
$$
0 = \nabla \cdot (\boldsymbol{\kappa}_{\mathrm{i}} \nabla \varphi_{\mathrm{m}}) + \nabla \cdot (\boldsymbol{\kappa}_{\mathrm{e}} + \boldsymbol{\kappa}_{\mathrm{i}}) \nabla \varphi_{\mathrm{e}} \quad \text{in } \Omega_{\mathbb{H}}
$$
$$
\frac{\partial \mathbf{s}}{\partial t} = \mathbf{g}(\varphi_{\mathrm{m}}, \mathbf{s}) \quad \text{in } \Omega_{\mathbb{H}}
$$
$$
0 = \nabla \cdot (\kappa_{\mathrm{b}} \nabla \varphi_{\mathrm{b}}) \quad \text{in } \Omega_{\mathbb{B}}
$$

with boundary conditions (BCs) at any time $t \in (0, T]$:

$$
\begin{array}{llll}
0 = (\boldsymbol{\kappa}_{\mathrm{i}} \nabla \varphi_{\mathrm{i}}) \cdot \mathbf{n} & \text{on } \partial \Omega_{\mathbb{H}} & \varphi_{\mathrm{e}} = \varphi_{\mathrm{b}} & \text{on } \partial \Omega_{\mathbb{H}} \cap \partial \Omega_{\mathbb{B}} \\
0 = (\kappa_{\mathrm{b}} \nabla \varphi_{\mathrm{b}}) \cdot \mathbf{n} & \text{on } \partial \Omega_{\mathbb{B}} \setminus \partial \Omega_{\mathbb{H}} & (\boldsymbol{\kappa}_{\mathrm{e}} \nabla \varphi_{\mathrm{e}}) \cdot \mathbf{n} = (\kappa_{\mathrm{b}} \nabla \varphi_{\mathrm{b}}) \cdot \mathbf{n} & \text{on } \partial \Omega_{\mathbb{H}} \cap \partial \Omega_{\mathbb{B}}
\end{array}
$$

together with admissible initial conditions and a cellular ionic model. We denote with $\boldsymbol{\kappa}_{\mathrm{i}}$ and $\boldsymbol{\kappa}_{\mathrm{e}}$ the intracellular and extracellular conductivity tensor fields, with

κ_b the torso conductivity, with $\varphi_m, \varphi_e, \varphi_b$ the transmembrane, extracellular, and body potential fields, with χ the volume to membrane surface ratio, and with C_m the membrane capacitance. In this work we have used the Mahajan's model for rabbit ventricular cardiomyocytes [11] as adopted in [9] for $\mathbf{g}$ and I_{ion}. Note that this formulation yields semi-definite forms. Therefore an additional Dirichlet BC $\varphi_b = 0$ on a non-empty subset of $\partial\Omega_\mathbb{B} \backslash \partial\Omega_\mathbb{H}$ is introduced (this BC can be loosely interpreted as a grounding). In this model, under the implicit assumption of no mechanical deformation, the ECG is simply the evaluation of φ_b over time at specific locations in $\Omega_\mathbb{B}$. We will refer to this ECG as the *direct ECG*.

2.2 Poisson Reconstruction

More widely used than the Bidomain model is the Monodomain model. Here the assumption $\kappa_i = \lambda\kappa_e$ is added to the previous system of equations to collapse the first two equations into one. Although it allows to simplify significantly the model, this assumption is rather problematic as all experimental observations suggest that $\kappa_i \neq \lambda\kappa_e$, see, e.g., [8]. Furthermore, this simplification raises the question on how to enforce the boundary conditions on the extracellular potential, as they are known to affect the electrical wave propagation at the boundary. We adopt the most commonly used approach and set the flux of the transmural potential across the heart's boundary equal to zero with a suitable conductivity tensor $\overline{\kappa}$ representing the conductivity in the Monodomain model:

$$\chi C_m \frac{\partial\varphi_m}{\partial t} = \nabla \cdot (\overline{\kappa}\nabla\varphi_m) - \chi I_{ion}(\varphi_m, \mathbf{s}) - \chi I_{stim}(t) \qquad \text{in } \Omega_\mathbb{H}$$

$$\frac{\partial\mathbf{s}}{\partial t} = \mathbf{g}(\varphi_m, \mathbf{s}) \qquad \text{in } \Omega_\mathbb{H}$$

$$0 = (\overline{\kappa}\nabla\varphi_m) \cdot \mathbf{n} \qquad \text{on } \partial\Omega_\mathbb{H}$$

With the solution of the Monodonain model we can reconstruct an approximate ECG as a postprocessing step by solving the following problem:

$$\nabla \cdot (\kappa_e + \kappa_i)\nabla\varphi_e = \underbrace{-\nabla \cdot (\kappa_i\nabla\varphi_m)}_{'=f'} \qquad \text{in } \Omega_\mathbb{H}$$

$$\nabla \cdot (\kappa_b)\nabla\varphi_b = 0 \qquad \text{in } \Omega_\mathbb{B}$$

$$0 = \varphi_b - \varphi_e \qquad \text{on } \partial\Omega_\mathbb{H} \cap \partial\Omega_\mathbb{B}$$

Because of its familiar structure, we name this approach *Poisson reconstruction* throughout this work.

2.3 Pseudo-ECG

Most studies using the Monodomain or Eikonal model reconstruct the ECG with a lead field approach [14] because it is less expensive to compute and it does not require an additional mesh for the surrounding torso. The ECG computed using

this approach is often refer to as *pseudo-ECG* and we adopt this convention here as well. A general integral form of the pseudo-ECG is given by:

$$\varphi_\mathrm{b}(\mathbf{x},t) \mapsto \frac{1}{4\pi\kappa_\mathrm{b}} \int_{\Omega_\mathbb{H}} \frac{\nabla \cdot \boldsymbol{\kappa}_\mathrm{i}(\tilde{\mathbf{x}})\nabla\varphi_\mathrm{m}(\tilde{\mathbf{x}},t)}{||\tilde{\mathbf{x}} - \mathbf{x}||_2} d\tilde{\mathbf{x}}, \tag{1}$$

where the original derivation assumes uniform, isotropic conductivity tensors. Moreover it is assumed that $\Omega_\mathbb{B}$ is a sphere with infinite radius and Dirichlet boundary condition $\varphi_\mathrm{b} = 0$ everywhere on the surface. Note that we introduced a modification to the formula, as we exchanged the commonly used bulk conductivity tensor with the intracellular conductivity tensor. This accounts for the intracellular anisotropic conductivity in the elliptic part of the Bidomain equation and is equivalent to 'f' in the Poisson reconstruction equations.

2.4   ECG Comparison: Similarity Measure

In order to quantitatively compare the morphology of computed ECGs, we adopt the PC^* correlation measure [12]. In contrast to the classic L_2 distance, the PC^* correlation measure is only sensitive to morphological differences – e.g., fractionations or spurious Q-waves – and not to differences in phase, amplitude, and duration.

2.5   Numerical Implementation

The Bidomain problem is solved by applying a Godunov operator splitting to separate the nonlinear cell model, containing the reaction term together with the system internal variables, from the linear system of partial differential equations (PDEs). The linear system of PDEs is solved using Rothe's method, where time is discretized via an implicit Euler scheme and space is discretized via the linear finite element method (see, e.g., [15]).

MFEM [1] is used as the numerical framework. The resulting linear system is solved via preconditioned conjugate gradient (PCG) method, where a block diagonal preconditioner combining HYPRE's [5] l1-scaled block SSOR for the first subsystem and BoomerAMG for the second subsystem is utilized. The discretization is finalized by applying an adaptive substepped explicit Euler scheme to the cell model as described in [10]. The Monodomain problem is solved following an analogous implementation, but using only a l1-scaled block SSOR preconditioner. The Poisson reconstruction is similarly implemented in MFEM and solved via PCG and BoomerAMG preconditioner. Default MFEM and HYPRE solver parameters have been adopted.

The used Monodomain and Bidomain solvers have been verified using the benchmark proposed in [13].

Equation 1 can be computed numerically using three approaches. A first possibility consists in using the *mass matrix method* (MMM) described in [4]. In this case, given φ_m, an auxiliary problem is solved for f:

$$f = \nabla \cdot \boldsymbol{\kappa}_\mathrm{i}(\tilde{\mathbf{x}})\nabla\varphi_\mathrm{m}(\tilde{\mathbf{x}},t),$$

and the pseudo-ECG is approximated by solving numerically

$$\varphi_{\rm b}(\mathbf{x}, t) \mapsto \frac{1}{4\pi\kappa_{\rm b}} \int_{\Omega_{\mathbb{H}}} \frac{f}{||\tilde{\mathbf{x}} - \mathbf{x}||_2} d\tilde{\mathbf{x}}.$$

The second approach is named *Gauss method* [6,9], since it relies on applying the Gauss theorem to Eq. 1. The boundary flux of the transmembrane potential is then set to zero (in agreement with the assumptions used in deriving the Monodomain model) leading to:

$$\varphi_{\rm b}(\mathbf{x}, t) \mapsto -\frac{1}{4\pi\kappa_{\rm b}} \int_{\Omega_{\mathbb{H}}} \boldsymbol{\kappa}_{\rm i}(\tilde{\mathbf{x}}) \nabla \varphi_{\rm m}(\tilde{\mathbf{x}}, t) \cdot \frac{\tilde{\mathbf{x}} - \mathbf{x}}{||\tilde{\mathbf{x}} - \mathbf{x}||_2^3} d\tilde{\mathbf{x}},$$

which is then evaluated numerically given $\varphi_{\rm m}$. This formulation can be interpreted as the projection of the electrical flux onto the scaled direction vectors pointing to the leads' positions [6].

A third possibility consists in evaluating directly Eq. 1, but is applicable only when $\varphi_{\rm m}$ is approximated using higher order interpolations (≥ 2).

3   Results

In this section we investigate the effect of the modeling assumptions on the ECG through numerical studies. We use the direct ECG as a reference, since the alternative approaches are derived from the full Bidomain model. We will analyze a simple "sphere in sphere" numerical setup and a biventricular model with a Purkinje network [9] embedded into a box torso to investigate the implications of alternative approaches to compute the ECG. In all numerical simulations a timestep equal to 0.01 ms is used, unless otherwise stated. Further we have set $C_m = 0.01 \, \mu\mathrm{F/mm}^2$ and $\chi = 140 \, /\mathrm{mm}$ in all experiments as chosen in [13].

3.1   Sphere in Sphere Numerical Setup

The first series of numerical experiments is constructed to satisfy as close as possible the original assumptions from which the lead field approach is formulated. Subsequently, we drop these assumptions individually to investigate their effect on the ECG. With this goal in mind, the active myocardium is modeled with a sphere embedded in a larger spherical domain representing the surrounding tissue as illustrated in Fig. 1. In one numerical test, a region with a lower conductivity is also introduced in the outer sphere to conceptually mimic the presence of the lungs. In order to ensure convergence, linear hexahedral elements with an average edge size of $200 \, \mu\mathrm{m}$ and $300 \, \mu\mathrm{m}$ have been used to discretize the active cardiac domain and the torso domain, respectively.

In the first experiment, we set $\kappa_{\rm b} = 0.2 \, \mathrm{mS/mm}$, $\boldsymbol{\kappa}_{\rm i} = \boldsymbol{\kappa}_{\rm e} = 0.2 \, \mathbf{I} \, \mathrm{mS/mm}$, and a zero Dirichlet BC on the surface of the outer sphere. The radius R of the outer sphere is varied from 12.5 mm to 25 mm and 50 mm to analyze convergence of the Poisson reconstruction approach toward the pseudo-ECG. The pseudo-ECG is
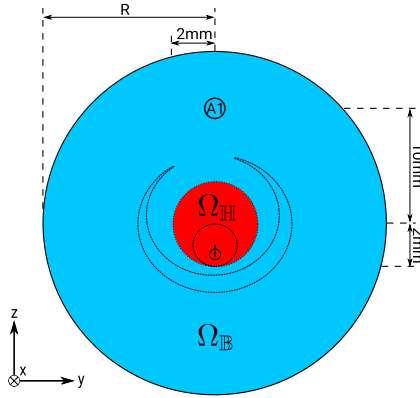
Fig. 1. "Sphere in sphere" numerical setup. An inner sphere centered at the origin with a radius of 2 mm models the heart. The inner sphere is embedded in a larger sphere, also centered at the origin and of radius R, which models the surrounding tissue. A spherical stimulus of $200\,\mu A/mm$ is applied at [0, 0, −1] for the first 1 ms of the simulation. The electrical field φ_b is measured at [0, 0, 10] in all numerical experiments. In the second numerical experiment, a C-shaped subdomain constructed by the set difference between a sphere of radius 4 mm centered at [0,0,0] and a smaller sphere of radius 3.25 mm centered at [0.00, 0.25, 0.75] is inserted in $\Omega_\mathbb{B}$. (Note that the representation of the numerical setup is not to scale.)

computed using both the Gauss method and Mass Matrix method. As illustrated in Fig. 2 (left), the ECG computed using the Poisson approach converges toward the pseudo-ECG as the radius of the outer sphere increases, therefore satisfying a key assumption in the derivation of the pseudo-ECG equation (Eq. 1). In this case, the Gauss method and Mass Matrix method lead to the same computed ECG. Although the MMM and Gauss methods do not always lead to exactly the same quantitative result, they always agree qualitatively in our experiments. Hence all the conclusions presented here hold and for simplicity only the Gauss method is used to compute the pseudo-ECG in the following.

The second series of experiments utilizes the same setup except the Monodomain model is exchanged with the Bidomain model and the Poisson reconstruction is replaced with the direct ECG. Similarly to the first experiment, the direct ECG converges toward the pseudo-ECG for increasing R (Fig. 2, right). However, a difference between the pseudo-ECG computed from the Monodomain model and the direct ECG still exist even for $R = 50.0$ mm. This difference is due the boundary flux of φ_e across $\partial\Omega_\mathbb{H}$, which was assumed to be zero.

Next the effect on the ECG of inhomogeneous conductivities in the surrounding tissue is investigated. For the next two experiments κ_b is set equal to 0.01 mS/mm (Fig. 3, left) and 0.05 mS/mm (Fig. 3, right) within the C-shaped region (see Fig. 1). Inhomogeneous conductivities may be due to the presence of different tissues such as the lungs and bones in a torso model. In this case we observe that the magnitudes of the direct and Poisson reconstructed ECGs are lower than the pseudo-ECG magnitude (Fig. 3).
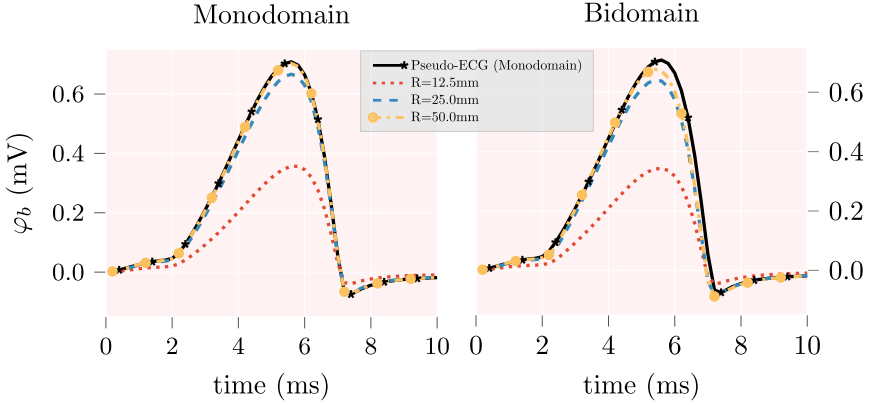
Fig. 2. Verification and validation of the pseudo-ECG formula with the Monodomain and Bidomain models using the setup from Fig. 1 with varying radius of the outer sphere and isotropic conductivity tensors $\kappa_i = \kappa_e = 0.2\,\mathbf{I}\,\mathrm{mS/mm}$ and $\kappa_b = 0.2\,\mathrm{mS/mm}$. Reference pseudo-ECGs were computed from the Monodomain solution. The Gauss and mass methods result in the same pseudo-ECG.
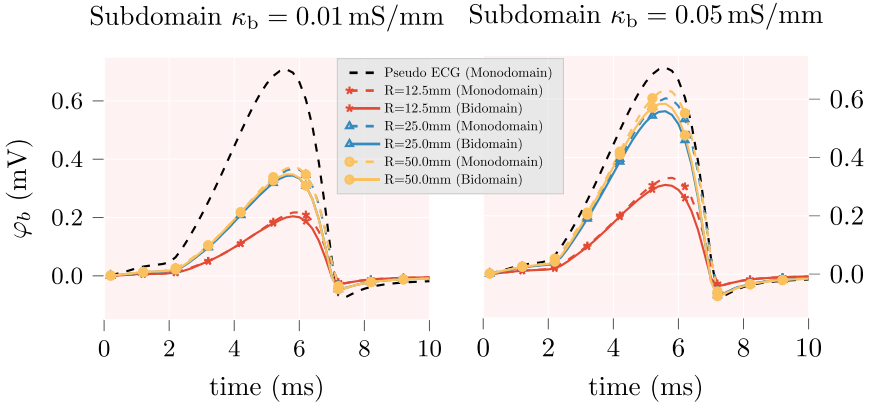

Fig. 3. ECG computed with inhomogeneous conductivities in $\Omega_{\mathbb{B}}$. All conductivities remain unchanged with respect to the previous experiment, except in the C-shaped subdomain (Fig. 1) where $\kappa_b = 0.01\,\mathrm{mS/mm}$ (left) and $\kappa_b = 0.05\,\mathrm{mS/mm}$ (right).

The subsequent set of experiments was designed to investigate the effect of the uniform and isotropic conductivity tensor assumption required to derive the pseudo-ECG approach, which is violated in realistic EP simulations. In all numerical experiments with an anisotropic conductivity tensor (uniform and non-uniform) the pseudo-ECG is not recovered for any sphere radius R with either the Poisson reconstruction or the direct ECG approach (Fig. 4).

In all numerical experiments involving the "sphere in sphere" numerical setup, the width of the ECG traces are nearly identical and the $PC*$

measures are all close to 1. The main differences are related to the magnitude of the pseudo-ECG compared to the ECG traces computed with the Poisson reconstruction or direct approach.
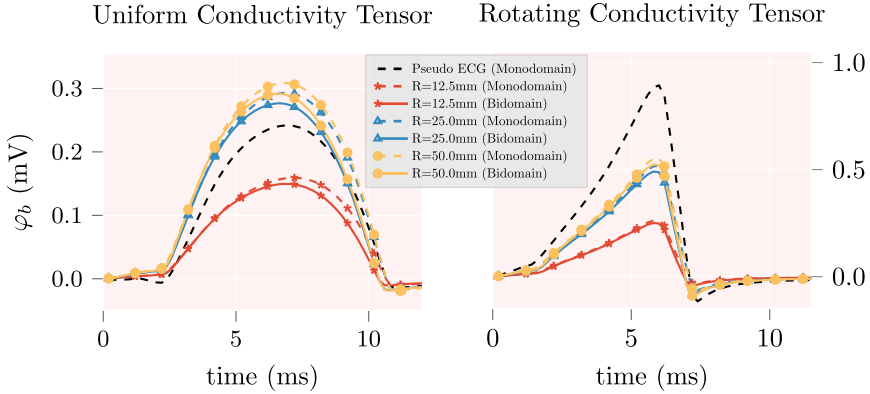

Fig. 4. ECG resulting from the setup illustrated in Fig. 1 with anisotropic uniform and non-uniform conductivity tensors. Solid lines represent Bidomain simulations and dashed lines Monodomain simulations. The eigenvalues of $\boldsymbol{\kappa}_i$ and $\boldsymbol{\kappa}_e$ are chosen as $[0.2, 0.1, 0.05]\,\mathrm{mS/mm}$ and $\kappa_b = 0.2\,\mathrm{mS/mm}$. In the uniform case (left) the eigenvectors are, in order, $[1, 0, 0]$, $[0, 1, 0]$, and $[0, 0, 1]$. In the non-uniform case, the second eigenvector is chosen along the radial direction, the third eigenvector along $[0,0,1]$, and the first eigenvector along the direction identified by the cross product of the second and third eigenvectors.

3.2   Biventricular Rabbit Model

Final experiments are conducted using a biventricular setup to investigate the effect of a more complex and realistic geometry together with more realistic boundary conditions. We have extended the rabbit biventricular model presented in [9] by embedding it in a box-shaped torso. Since we only investigate antero-grade propagation from the Purkinje network in the healthy case, the activation sequence is precomputed via Dijkstra's algorithm as presented in [17]. Accordingly, a short stimulus of $250\,\mu\mathrm{A/mm}$ is applied for $4\,\mathrm{ms}$ to all nodes in a search radius equal to $300\,\mu\mathrm{m}$ from the activated Purkinje muscle junctions. Here we use a timestep of $0.05\,\mathrm{ms}$.

The ECG is computed using the Wilson leads located in the same positions as in [9] (see also Fig. 5). The ground electrode boundary condition is applied to the face closest to the subject right foot. The first experiment uses an isotropic conductivity tensor and focuses on the effect of boundary conditions and heart geometry. The second experiment includes an anisotropic conductivity tensor [7] in combination with the original experimentally measured myofiber, sheetlet, and normal directions to investigate the discrepancies in a real case scenario between pseudo-ECG and direct or Poisson-reconstructed ECGs. Direct ECG
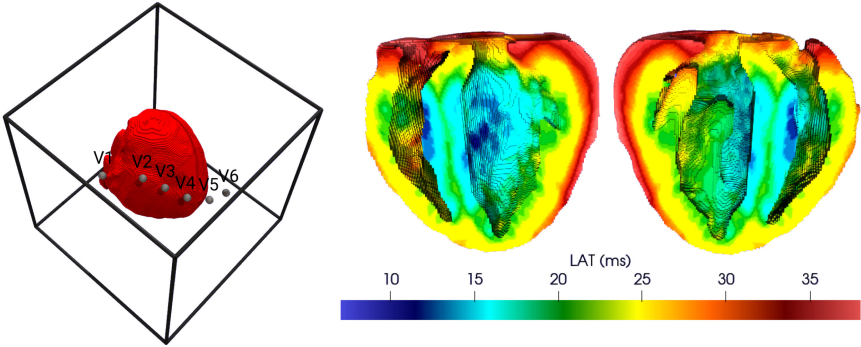
Fig. 5. Left: experimental setup with the heart embedded into a box torso of dimension 51.2 mm × 51.2 mm × 51.2 mm aligned with the biventricular model longitudinal axis. The Wilson leads' placement with respect to the biventricular model is also shown. Right: open biventricular view of the activation maps obtained in the Bidomain simulation with anisotropic conductivity tensors.

traces and ECG computed via Poisson reconstruction present the same overall features and progression. In contrast, the pseudo-ECG presents larger and lead-dependent discrepancies with respect to the direct ECG (Fig. 6). Results of the correlation analysis are reported in Table 1.

Table 1. Generalized Pearson correlation coefficients comparing the ECG computed in the isotropic and anisotropic biventricular simulations using the lead field method (pseudo-ECG), the Poisson reconstruction, and the direct approach.

		V1	V2	V3	V4	V5	V6
Isotropic	$PC^*_{\text{direct, pseudo}}$	0.838	0.930	0.941	0.921	0.907	0.932
	$PC^*_{\text{Poisson, pseudo}}$	0.910	0.943	0.936	0.931	0.919	0.940
	$PC^*_{\text{Poisson, direct}}$	0.947	0.931	0.930	0.945	0.961	0.979
Anisotropic	$PC^*_{\text{direct, pseudo}}$	−0.039	0.416	0.703	0.855	0.922	0.976
	$PC^*_{\text{Poisson, pseudo}}$	−0.247	0.244	0.772	0.940	0.963	0.976
	$PC^*_{\text{Poisson, direct}}$	0.989	0.985	0.989	0.995	0.996	0.997

4 Discussion

The first set of numerical experiments using the spherical setup confirmed that the widely used pseudo-ECG agrees with the Poisson reconstruction approach when an isotropic uniform conductivity tensor is adopted and for large enough surrounding domains. In this ideal case the ECG computed using the Monodomain model can be reconstructed using either approach. However, further experimentation on the idealized spherical setup, revealed that the hypothesis
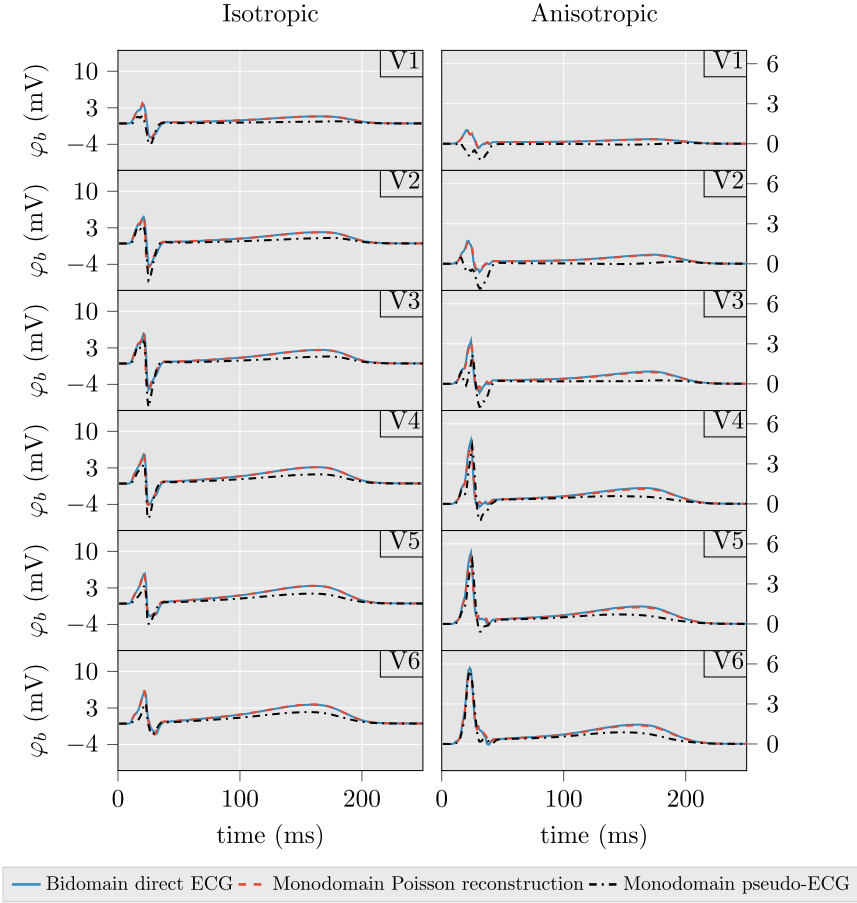
Fig. 6. Precordial ECG computed from EP simulations on a rabbit heart. Left: uniform, isotropic conductivity tensor $(0.2\,\mathbf{I}\,\mathrm{mS/mm})$. Right: full model as in [9] with Hooks' conductivities [7]. For the Monodomain simulation we have chosen $\overline{\boldsymbol{\kappa}} = 0.5\,\boldsymbol{\kappa}_{\mathrm{i}}$. Note that κ_{b} has been set equal to 0.2 mS/mm in these simulations.

of uniform isotropic conductivity tensor is essential for the pseudo-ECG to be accurate. As soon as an inhomogeneous surrounding domain or an anisotropic conductivity tensor – uniform or non-uniform over the inner sphere – is introduced, the pseudo-ECG approach leads to traces that only qualitatively agree with the direct ECG, i.e., their morphology is similar but their magnitude differs. In comparison, the Poisson reconstruction leads to results which remain quantitatively closer to the direct ECG.

Discrepancies between the pseudo-ECG and the direct ECG increase in a biventricular setup embedded in a homogeneous domain representing an idealized torso. In this case, the pseudo-ECG does not approximate the direct ECG qualitatively well in some of the Wilson leads, e.g., V1 and V2 in the anisotropic

case as shown in Fig. 6 and by the PC^* measures in Table 1 being far from one. This discrepancy may be due to the complex geometry and strongly anisotropic conductivities in the biventricular simulations, which were not captured by the "sphere in sphere" experiment.

In all experiments, the ECG computed using the Poisson reconstruction approach is similar to the direct ECG. The remaining differences are likely due to the boundary flux of φ_e across $\partial\Omega_{\mathbb{H}}$, which was assumed to be zero in the Monodomain model. This missing boundary term can be resolved adopting the pseudo-Bidomain approach [2], which we plan to address in future work.

We conclude by noting some of the limitations of the current study. First, only a few cases are considered in the "sphere in sphere" experimental setup. These are likely not sufficient to pinpoint all major discrepancies between the pseudo-ECG and the direct or Poisson reconstructed ECGs. Second, we did not investigate the effect of different conductivity values on the ECGs computed with the presented methods and their similarity measures. Third, we emphasize that further refinement of the biventricular Bidomain model is needed to replicate a physiologically accurate ECG with the conductivity tensor employed in this study. In this context, the discrepancies between the Monodomain and Bidomain experiments in the biventricular setup could be due, at least in part, to the sub-optimal choice of the conductivity tensor for the Monodomain simulation. Finally, the current study was focused on the Wilson leads and did not analyze the possible discrepancies among methods in computing other electrodes' arrangements, such as the Einthoven leads' placement.

Based on the current results, we recommend that the Poisson reconstruction approach is selected in cardiac EP simulations based on the Monodomain model where obtaining a more accurate ECG is important. In all the numerical experiments reported herein, the computational cost associated with the Poisson reconstruction approach was only slightly higher than the cost required by the pseudo-ECG approach. Although no careful optimization of the numerical implementation has been carried out and the torso model employed here is small, these preliminary results suggest that the Poisson reconstruction is a viable solution to efficiently and accurately compute the ECG.

References

1. Anderson, R., et al.: MFEM: a modular finite element library. Comput. Math. Appl. **81**, 42–74 (2020)
2. Bishop, M.J., Plank, G.: Bidomain ECG simulations using an augmented monodomain model for the cardiac source. IEEE Trans. Biomed. Eng. **58**(8), 2297–2307 (2011)
3. Boulakia, M., Cazeau, S., Fernández, M.A., Gerbeau, J.F., Zemzemi, N.: Mathematical modeling of electrocardiograms: a numerical study. Ann. Biomed. Eng. **38**(3), 1071–1097 (2010)
4. Dupraz, M., Filippi, S., Gizzi, A., Quarteroni, A., Ruiz-Baier, R.: Finite element and finite volume-element simulation of pseudo-ECGs and cardiac alternans. Math. Methods Appl. Sci. **38**(6), 1046–1058 (2015)

5. Falgout, R.D., Yang, U.M.: *hypre*: a library of high performance preconditioners. In: Sloot, P.M.A., Hoekstra, A.G., Tan, C.J.K., Dongarra, J.J. (eds.) ICCS 2002. LNCS, vol. 2331, pp. 632–641. Springer, Heidelberg (2002). https://doi.org/10.1007/3-540-47789-6_66

6. Göktepe, S., Kuhl, E.: Computational modeling of cardiac electrophysiology: a novel finite element approach. Int. J. Numer. Methods Eng. **79**(2), 156–178 (2009)

7. Hooks, D.A., Trew, M.L., Caldwell, B.J., Sands, G.B., LeGrice, I.J., Smaill, B.H.: Laminar arrangement of ventricular myocytes influences electrical behavior of the heart. Circ. Res. **101**(10), e103–e112 (2007)

8. Johnston, B.M., Johnston, P.R.: Approaches for determining cardiac bidomain conductivity values: progress and challenges. Med. Biol. Eng. Comput. **58**(12), 2919–2935 (2020). https://doi.org/10.1007/s11517-020-02272-z

9. Krishnamoorthi, S., et al.: Simulation methods and validation criteria for modeling cardiac ventricular electrophysiology. PloS one **9**(12), e114494 (2014)

10. Krishnamoorthi, S., Sarkar, M., Klug, W.S.: Numerical quadrature and operator splitting in finite element methods for cardiac electrophysiology. Int. J. Numer. Methods Biomed. Eng. **29**(11), 1243–1266 (2013)

11. Mahajan, A., et al.: A rabbit ventricular action potential model replicating cardiac dynamics at rapid heart rates. Biophys. J. **94**(2), 392–410 (2008)

12. Mincholé, A., Zacur, E., Ariga, R., Grau, V., Rodriguez, B.: MRI-based computational torso/biventricular multiscale models to investigate the impact of anatomical variability on the ECG QRS complex. Front. Physiol. **10**, 1103 (2019)

13. Niederer, S.A., et al.: Verification of cardiac tissue electrophysiology simulators using an N-version benchmark. Philos. Transa. R. Soc. A Math. Phys. Eng. Sci. **369**(1954), 4331–4351 (2011)

14. Plonsey, R., Barr, R.C.: Bioelectricity: A Quantitative Approach. Springer, New York (2007). https://doi.org/10.1007/978-0-387-48865-3

15. Sundnes, J., Lines, G.T., Cai, X., Nielsen, B.F., Mardal, K.A., Tveito, A.: Computing the Electrical Activity in the Heart, vol. 1. Springer, Heidelberg (2007). https://doi.org/10.1007/3-540-33437-8

16. Tung, L.: A bi-domain model for describing ischemic myocardial D-C potentials. Ph.D. thesis, Massachusetts Institute of Technology (1978)

17. Wallman, M., Smith, N.P., Rodriguez, B.: A comparative study of graph-based, eikonal, and monodomain simulations for the estimation of cardiac activation times. IEEE Trans. Biomed. Eng. **59**(6), 1739–1748 (2012)